Hindawi
Wireless Communications and Mobile Computing
Volume 2021, Article ID 8164367, 14 pages
https://doi.org/10.1155/2021/8164367

Research Article

The Potential of Massive-MIMO on TV Towers for Cellular Coverage Extension

Tayebeh Taheri, Rickard Nilsson, and Jaap van de Beek

Department of Computer Science, Electrical and Space Engineering, Luleå University of Technology, SE 971 87 Luleå, Sweden

Correspondence should be addressed to Jaap van de Beek; jaap.vandebeek@ltu.se

Received 13 December 2019; Revised 13 December 2020; Accepted 7 January 2021; Published 22 January 2021

Academic Editor: Heikki Karvonen

Because of low potential revenue, network operators have mainly focused on providing connectivity in urban areas rather than in rural areas resulting in technology improvement in favour of urban areas; and consequently, most of remote areas suffer from poor or lack of connectivity. In this paper, we present the potential of massive-MIMO to provide connectivity to sparse areas. We show that we can cover large rural areas with radius of tens of km using massive-MIMO mounted on existing infrastructure of TV towers. We also show that, in contrast with common belief, higher frequencies, e.g., 3500 MHz rather than 700 MHz, can reach farther utilizing massive-MIMO, provided that the antenna area is the same.

1. Introduction

By the evolution of cellular devices from Nordic mobile telephony (NMT) to nowadays 5G cellular devices, connectivity has improved in many aspects but not in signal range (signal power). In 1981, the first fully automatic cellular phone systems, NMT, with the frequency range of 450 MHz were introduced. High-power NMT transmission could cover large areas. Demand for a higher bit-rate in all parts of the network has been increased during years. To provide higher data-rate to the users, which are located mostly in urban areas, GSM, 3G, and 4G focused more on higher and higher frequencies and smaller cell size. Even though the low-frequency bands have been used in all generations, this usage has not been developed enough to provide demanded connectivity to far distances including sparse areas. Wireless systems have tackled the coverage problem by building more and more base stations and splitting large areas into small cells (smaller areas). The focus has been mainly on urban areas, roads, and railways, since building base stations or dig fibre to cover the sparse areas is too expensive.

By the end of 2020, more than eight billion devices will be connected to 5G technology [1], where most of the subscribers are in urban and suburban areas. Even though connectivity is part of social justice, it is one of the significant impairments in the United Nation's sustainable development goals (SDG) [2, 3]. Because of low potential revenue, network operators have been reluctant to invest in providing connectivity to rural areas resulting in technology improvement, in favour of the urban areas leaving the remote areas without connectivity.

In recent years, the demand for connectivity in remote areas has been shifting from end-consumers to industry and society. The European Commission has declared the goal that all EU-citizens will have access to the internet speed of 30 Mbits/s by the year 2020. However, just in Sweden, 7-10 percent of citizens, mainly live in rural and sparse areas in the north, do not have access to it yet [4]. It means over 700,000 people in Sweden are potentially excluded.

Several solutions have been proposed to provide internet connectivity to rural areas, to mention some, Google balloons [5, 6], unmanned aerial vehicles (UAVs) [7, 8], satellite [9], and very recently, using sectorized antennas located on TV towers [10].

Google has proposed the use of balloons called as Loon project to cover radius of around 20 km in rural areas [6]. Base station equipments as well as solar panels to provide energy and a lithium battery to save the solar energy are mounted on each balloon. Not only use of solar panels is critical especially in wintertime in northern countries such as

Sweden, each balloon needs physical maintenance such as caring the envelope or replacing the gas cylinder, which controls the altitude, every now and then. A Loon balloon can work only 100 days [6]. There are two types of communication in Loon balloons, balloon to balloon and balloon to ground. Multiple balloons need to get connected to each other in a chain to deliver the connectivity to faraway users (balloon to balloon communication). Moreover, since balloons are moving constantly, each user has to track the balloons continuously [5]. With all being said, continuous connection is challenging by Loon balloons.

Another proposed solution to provide connectivity to rural areas is to use base stations carried by Unmanned Aerial Vehicles (UAVs) [7, 8]. The use of UAVs is limited in terms of time, required planning algorithm, and energy consumption and is also challenging in sophisticated and violated environments. UAVs are promising in temporary use such as emergency situations, but it fails in providing the permanent connectivity to households in sparse areas.

A very recent study proposes using a stack of sector antennas on a TV tower and designs the antennas in order to make a high power narrow beam which can reach farther away [10].

Some studies have suggested to use satellite communication for hard-to-reach areas [9]. Satellite communication is another promising technology for obtaining full coverage, but it is beyond the scope of this paper to compare with this technology.

Massive-MIMO is usually used in urban scenarios to increase the capacity in urban small cells. The mentioned solutions for rural connectivity including UAVs and sector antennas have been investigated in the literature to some extent. Complementary to these studies, the potential of terrestrial networks to serve large rural areas needs further investigation since such networks, equipped with the latest emerging antenna technologies potentially could provide low-cost economically attractive alternatives. In this paper, we study the feasibility of providing connectivity to sparse areas utilizing massive-MIMO. We use the existing infrastructure of TV towers, see Figure 1, to avoid the costly building of new infrastructure (building of new base stations or optical fibres). We show that we can cover a radius of 70 km around a TV tower with the speed of 30 Mbits/s using massive-MIMO technology. We also show that higher speed and/or larger areas coverage is possible under some assumptions such as antenna diversity or dropping the worst conditioned users. The proposed solution is scalable and deploys minimum infrastructure. We also show that, in contrast with the common belief that a lower frequency is more proper for reaching far distances, higher frequencies provide larger area coverage, provided that the antenna array area is the same.

In this paper, we follow the approach in [11, 12] and assume that antenna elements experience independent Rayleigh fading channels. Even though this assumption is optimistic but gives us the analytical expression needed to find the upper bound results.

The paper continues as follows. In Section II, we introduce the system model and notation. In Section III, we discuss the base station antenna array area as the main cost to provide connectivity. We evaluate the requirements to achieve the target uplink and downlink throughput in Section IV. We also discuss the impact of dropping the worst conditioned users on the system throughput. Finally, Section V concludes the paper.

2. System Model

In this paper, for simplicity, we assume a single cell and we investigate the maximum area we can cover using a single TV tower. However, for full coverage, more cells and towers are required. This is beyond the scope of this paper and is a subject of future research.

We consider a single-cell base station with M number of antennas serving U user and look at the transmitted and received signals both on the uplink and downlink. We assume the noise samples, both in uplink and downlink, are i.i.d. Gaussian distributed $\mathcal{CN}(0, 1)$.

In this paper, we assume omnidirectional antenna elements, both at the transmitter and receiver sides. The use of other types of antennas such as directive antennas may reduce the number of required antenna elements. In this paper, we assume the subscribers are static (households); however, the use of omnidirectional antennas enables the proposed structure to be extended to provide connectivity to mobile users in a simpler way rather than using other types of antennas.

In this paper, we consider time division duplex (TDD) systems where the uplink and downlink use the same frequency spectrum but different time slots. Channel is estimated on uplink transmission from received pilot signals from U users. The channel estimated at the base station in the uplink is used to form the transmit signal in the downlink.

2.1. Uplink. In the uplink, U terminals weight their respective symbols, d_u, by power coefficient η_u $(0 \le \eta_u \le 1)$ as

$$s_u = \sqrt{\eta_u} d_u, \tag{1}$$

and then synchronously send them to the base station

$$\mathbf{s} = \mathbf{D}_{\eta}^{\frac{1}{2}} \mathbf{d}, \tag{2}$$

where $\mathbf{s} = [s_1, \cdots, s_U]^T$ is the normalized transmitted signal vector, $\eta = [\eta_1, \cdots, \eta_U]^T$, $\mathbf{D}_\eta$ is the diagonal matrix with the elements of η on its diagonal, and $\mathbf{d} = [d_1, \cdots, d_U]^T$ is the uncorrelated data symbol with zero mean and unit variance, $E\{\mathbf{d}\mathbf{d}^H\} = \mathbf{I}_U$.

At the base station, the received signal vector, $\mathbf{r}$, is

$$\mathbf{r} = \sqrt{\rho_{ul}} \mathbf{H}\mathbf{s} + \mathbf{n}, \tag{3}$$

where $\mathbf{r} = [r_1, \cdots, r_M]^T$, $\mathbf{n} = [n_1, \cdots, n_M]^T$ is the receiver noise vector and ρ_{ul} denotes the average uplink signal-to-noise ratio (SNR). Matrix $\mathbf{H}$ represents the channel propagation

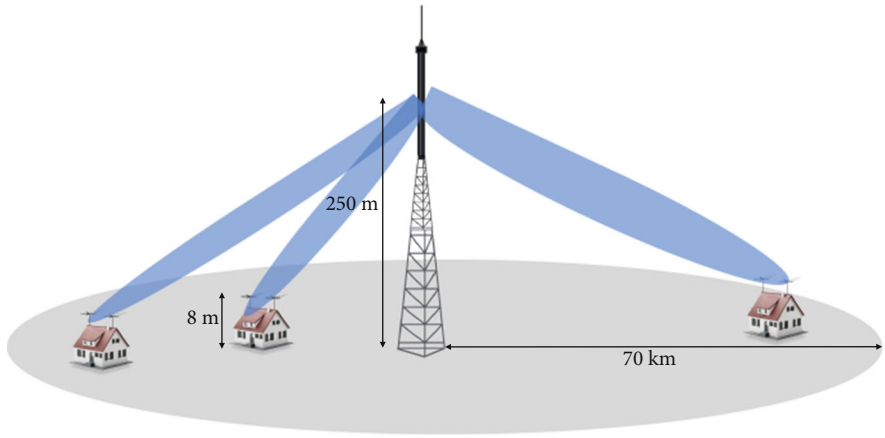

Figure 1: A simplified illustration of coverage in sparse areas using massive-MIMO antennas mounted on a TV tower.

matrix between the M base station antennas and the U users,

$$\mathbf{H} = \begin{bmatrix} h_{1,1} & h_{1,2} & \cdots & h_{1,U} \\ h_{2,1} & h_{2,2} & \cdots & h_{2,U} \\ \vdots & & \ddots & \vdots \\ h_{M,1} & h_{M,2} & \cdots & h_{M,U} \end{bmatrix}, \quad (4)$$

where $h_{m,u}$ is scalar and represents the channel coefficient between the uth user and mth BS antenna.

Later received signal r is decoded at the base station,

$$\mathbf{G}_{\text{dec}}^{H}\mathbf{r} = \mathbf{G}_{\text{dec}}^{H}(\sqrt{\rho_{ul}}\mathbf{H}\mathbf{s} + \mathbf{n}), \quad (5)$$

where $\mathbf{G}_{\text{dec}}$ represents the decoder. In massive-MIMO linear processing such as Zero-Forcing (ZF) and Maximum-Ratio (MR) are near optimal for decoding the uplink received signal, $\mathbf{r}$, [11].

2.2. Downlink. The downlink transmit vector, $\mathbf{s} = [s_1, \cdots, s_M]^T$, is generated by first scaling the date symbols $\mathbf{d} = [d_1, \cdots, d_U]^T$ using the downlink power control coefficients, η_u $(0 \le \sum_{u=1}^{U}\eta_u = 1)$, and then, in order to avoid multiuser-interference and increase the capacity of the MIMO system, the downlink transmit signal is precoded at the base station using a size $M \times U$ precoding matrix $\mathbf{G}_{\text{pre}}$ [11].

$$\mathbf{s} = \mathbf{G}_{\text{pre}}\mathbf{D}_{\eta}^{\frac{1}{2}}\mathbf{d} = \sum_{u=1}^{U}\sqrt{\eta_u}\mathbf{g}_u d_u, \quad (6)$$

where $\mathbf{g}_u$ is the uth column of $\mathbf{G}_{\text{pre}}$. Received signal on terminal u, r_u, is

$$r_u = \sqrt{\rho_{dl}}\mathbf{h}_u\mathbf{s} + n_u, \quad (7)$$

where n_u is the uth receiver noise, $\mathbf{h}_u = [h_{1,u}, \cdots, h_{M,u}]$, and ρ_{dl} denotes the average downlink SNR. In the downlink, the channel matrix is $\mathbf{H}^T$ which is the transpose of the uplink channel matrix in (4); this is because of the reciprocity assumption in the massive-MIMO systems, where $\mathbf{n} = [n_1, \cdots, n_U]^T$ is the receiver noise vector and ρ_{dl} denotes the average downlink SNR. In (7), channel matrix $\mathbf{H}^T$ is the transpose of the uplink channel matrix in (4); this is because of the reciprocity assumption in the massive-MIMO systems.

In downlink massive-MIMO, similar to uplink, linear processing such as ZF and MR is near optimal for the downlink precoding [11].

Throughout this paper, we assume ZF linear processing for both uplink decoding and downlink precoding. On the downlink, we choose $\mathbf{G}_{\text{pre}} = \mathbf{G}^{\text{ZF}}$ and on the uplink we choose $\mathbf{G}_{\text{dec}} = \mathbf{G}^{\text{ZF}}$, where

$$\mathbf{G}^{\text{ZF}} = \left(\mathbf{H}^{H}\mathbf{H}\right)^{-1}\mathbf{H}^{H}. \quad (8)$$

2.3. Channel Assumptions. Every channel matrix elements $h_{m,u}$ in (4) captures components of channel response via a large scale fading coefficient, β_u and a small-scale fading coefficient, $\tilde{h}_{m,u}$ as

$$h_{m,u} = \sqrt{\beta_u}\tilde{h}_{m,u}. \quad (9)$$

We assume that small-scale fading is independent Rayleigh, $\tilde{h}_{m,u}$ is i.i.d $\mathcal{CN}(0,1)$. This is an optimistic assumption which allows us to borrow the analytical expression from [11, 12]. The study of other channels with different distributions is a subject for future investigations. Considering independent Rayleigh fading channel gives us the upper bound results. Owing to ZF processing the effect of $\tilde{h}_{m,u}$ disappears (channel hardening) [11].

Large scale fading coefficient (β_u) includes the path-loss and shadow fading. There are several path-loss Models in the literature, including Ericsson 9999 [13] and Hata [14]. In particular, here, we look at the Ericsson 9999 rural model. Ericsson 9999 model is an extension of Hata model (frequency range of 150-1500 MHz) for higher frequencies; and

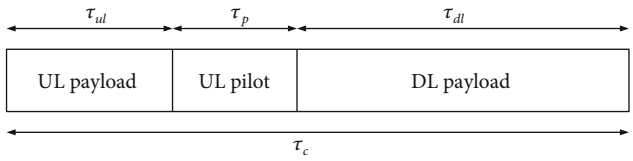

Figure 2: Coherence block allocation in massive-MIMO.

in the literature, it has been used for frequencies of up to 3.5 GHz [13]. In Ericsson 9999 model, path-loss, in dB, on uth user is

$$\begin{aligned}\mathrm{PL}_u = -\big(&36.2 + 30.7\log 10(d) - 12\log 10(h_{tx}) \\ &+ 0.1\log 10(h_{tx})\log 10(d) - 3.2(\log 10(11.75h_{rx}))^2 \\ &+ 44.49\log 10(f_c) - 4.78(\log 10(f_c))^2\big),\end{aligned} \tag{10}$$

where d is the distance between the uth user and the base station in km, h_{tx} is the base station tower height in meter, h_{rx} is the user's antenna height in meter, and f_c is the carrier frequency in MHz.

On top of path-loss, we consider the log-normal shadow fading effect, $SF_u \sim \mathcal{LN}(0, 8)$. The large scale fading coefficient, β_u becomes

$$\beta_u = 10^{(PL_u - SF_u)/10}, \tag{11}$$

where SF_u represents the shadow fading on uth user's antenna.

The large scale fading coefficient, β_u, is assumed to be constant over a time-frequency block called coherence block [11]. The time-frequency resources are divided into blocks of size B_c Hz and T_c s, with the purpose of making each user channel approximately frequency-flat and static within a block. Hence, the bandwidth B_c is selected to be smaller or equal to the anticipated channel coherence bandwidth among the users, while T_c is smaller or equal to the anticipated channel coherence time of the users. Each block is referred to as a coherence block. Due to the Nyquist-Shannon sampling theorem, the number of transmission symbols that fit into a coherence block is given by

$$\tau_c = T_c B_c. \tag{12}$$

Coherence bandwidth, B_c, can be calculated as

$$B_c \approx \frac{1}{2\pi\sigma_\tau}, \tag{13}$$

where σ_τ is the rms delay spread. In rural area, median rms delay spread is around $0.1\mu s$ [15]; however, in this paper, we use a more conservative value of $B_c = 1000$ kHz.

Coherence time, T_c, is a function of user speed as [16]

$$T_c = \frac{1}{f_m} = \frac{c}{v f_c}, \tag{14}$$

Table 1: Number of antennas that fits in each column-array in different carrier frequencies of f_c assuming area of a cylinder with radius of $r = 2$ m and heigh of h.

	$f_c = 700$ MHz	$f_c = 1800$ MHz	$f_c = 3500$ MHz
$A = 40\,\mathrm{m}^2 (h \approx 3.2\mathrm{m})$	28	76	148
$A = 100\,\mathrm{m}^2 (h \approx 8\mathrm{m})$	74	190	370
$A = 125\,\mathrm{m}^2 (h \approx 10\mathrm{m})$	92	238	464

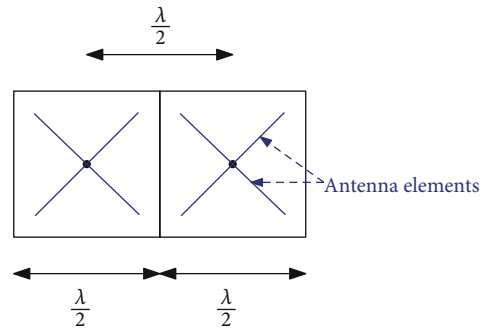

Figure 3: One possible antenna elements configuration.

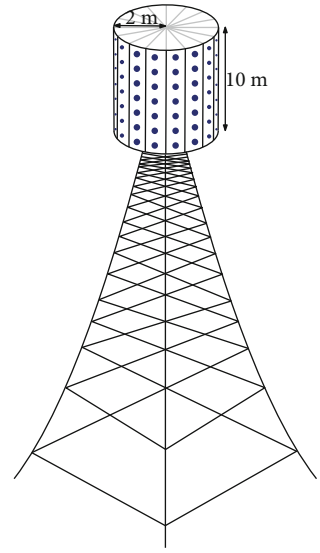

Figure 4: A cylindrical antenna array with $A \approx 125\,\mathrm{m}^2$.

where f_m is the maximum Doppler shift, c is the light speed, v is the user speed, and f_c is the carrier frequency. In this paper, we aim at providing connectivity to fixed households; however, in our evaluations in Section IV, we use a more conservative value of $v = 2$ km/hr.

In massive-MIMO, the coherence block τ_c is split in three portions of uplink payload τ_{ul}, uplink pilot sequence τ_p, and downlink payload τ_{dl} as shown in Figure 2.

2.4. Spectral Efficiency and Throughput. The effective rigorous signal-to-interference-plus-noise ratio (SINR) for the u th terminal, SINR_u, in case of independent Rayleigh fading

Table 2: Summary of used parameters.

Base station antenna gain	0 dBi
Terminal antenna gain	6 dBi
Base station receiver noise figure	9 dB
Terminal receiver noise figure	9 dB
Nominal noise temperature	300 K
Radiated uplink power per terminal	31 dBm (Class-1 HPUE)
Total radiated downlink power	51.7 dBm (150 W)
Carrier frequency	700, 1800, 3500 MHz
Spectral BW	20 MHz
Density (number of households per km^2)	0.15 [20]
Terminal mobility	2 km/hr
Coherence BW	1000 kHz
Shadow fading standard deviation	8 dB
Shadow fading diversity	One antenna, best of two antennas
Path loss model	Ericsson 9999
Terminal antenna height	8 m
Base station antenna height	250 m (antenna array with length of 2x (in meter) is mounted on the height between $250 - x$ and $50 + x$ (in meter))

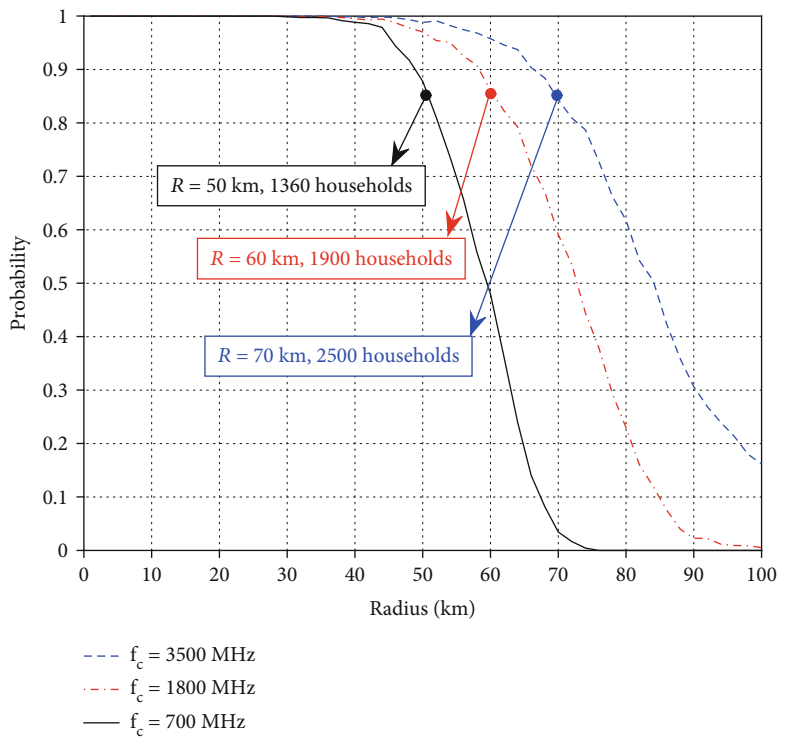

Figure 5: Probability of 15 Mbits/s uplink throughput for all users located within a radius of R.

channel and assuming ZF processing is [11]

$$SINR_u^{UL} = \frac{(M-U)\rho_{ul}\gamma_u\eta_u^{ul}}{1+\rho_{ul}\sum_{u'=1}^{U}\left(\beta_u{}' - \gamma_u{}'\right)\eta_{u'}^{ul}}, \quad (15)$$

$$SINR_u^{DL} = \frac{(M-U)\rho_{dl}\gamma_u\eta_u^{dl}}{1+\rho_{dl}(\beta_u-\gamma_u)\sum_{u'=1}^{U}\eta_{u'}^{dl}}, \quad (16)$$

where γ_u is the mean-square of the channel estimate. η_u^{ul} is the uplink power control coefficient satisfying $0 \le \eta_u^{ul} \le 1$,

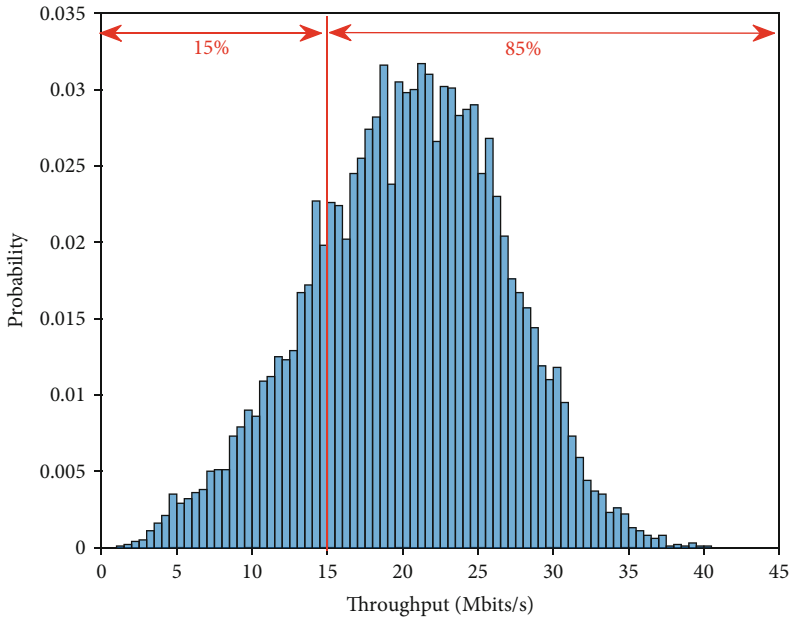

FIGURE 6: The probability histogram for throughput of users within the radius of $R = 60$ km where $f_c = 1800$ MHz.

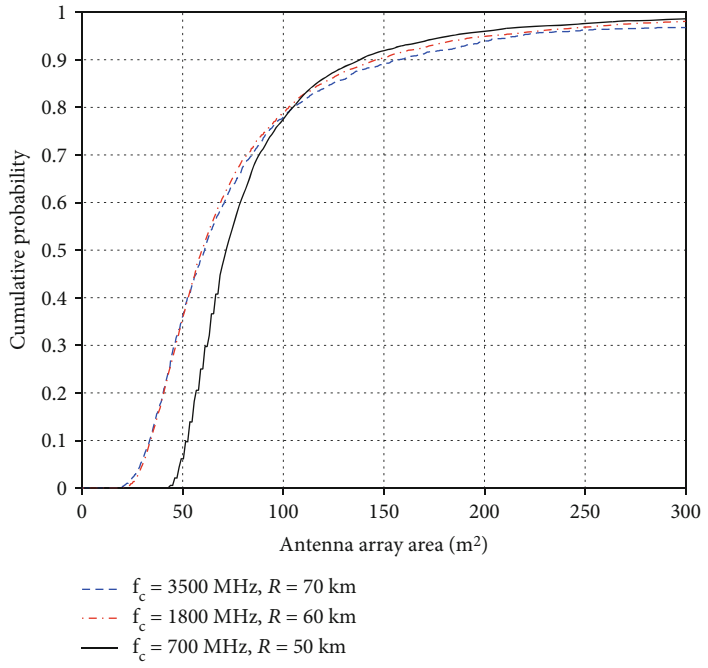

FIGURE 7: The probability of achieving uplink throughput of 15 Mbits/s/terminal for antenna array area of A.

and η_u^{dl} is the downlink power control coefficient satisfying $0 \le \eta_u^{dl}$ and $\sum_{u=1}^{U} \eta_u^{dl} \le 1$; ρ_{ul} and ρ_{dl} are calculated using link budget calculation considering $\beta_u = 1$.

The effective SINR values in (15) and (16) determine the lower bounds on (ergodic) sum capacity, C, as

$$C = E\left\{\sum_{u=1}^{U} C_{\text{inst},u}\right\} \ge E\left\{\sum_{u=1}^{U} \log_2(1 + SINR_u)\right\}, \quad (17)$$

where $C_{\text{inst},u}$ represents the instantaneous capacity on uth user. Sum capacity, (17), is only used in the optimization process in Section IV to find the minimum number of required antennas.

The (ergodic) sum spectral efficiency is

$$\text{Spectral efficiency} = \alpha C, \quad (18)$$

where on the uplink $\alpha = \tau_{ul}/\tau_c$ and on the downlink $\alpha = \tau_{dl}/\tau_c$. Here, τ_c is the total available samples in the coherence block,

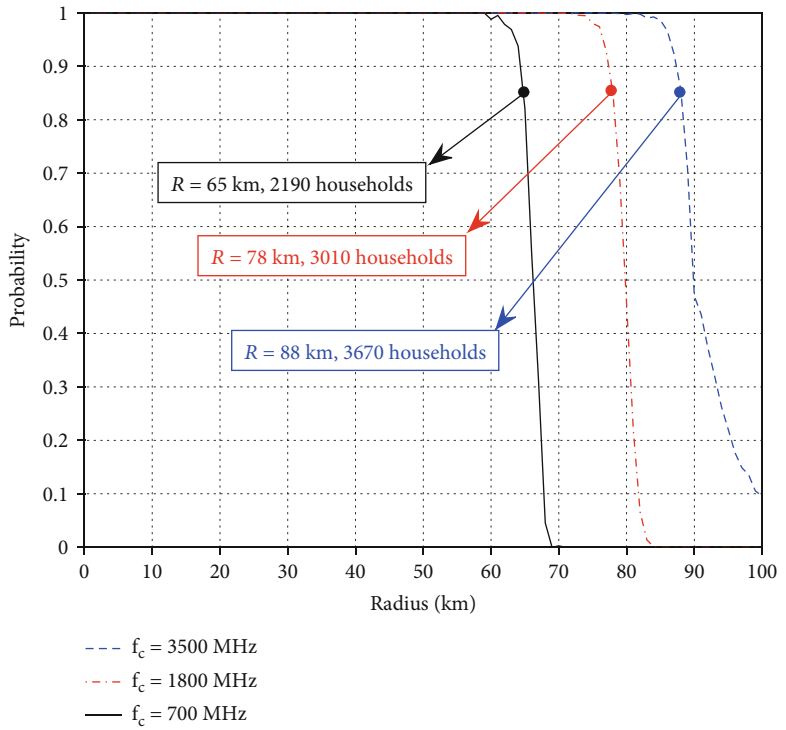

Figure 8: Probability of downlink throughput of 30 Mbits/s/terminal on all users located within a radius of R.

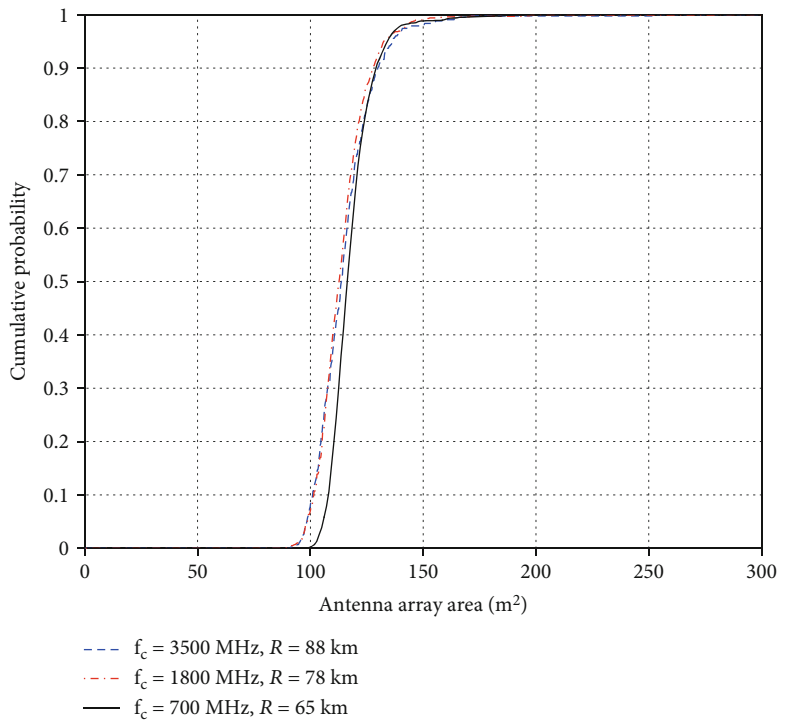

Figure 9: Probability of delivering downlink throughput of 30 Mbits/s/terminal utilizing antenna array area of A.

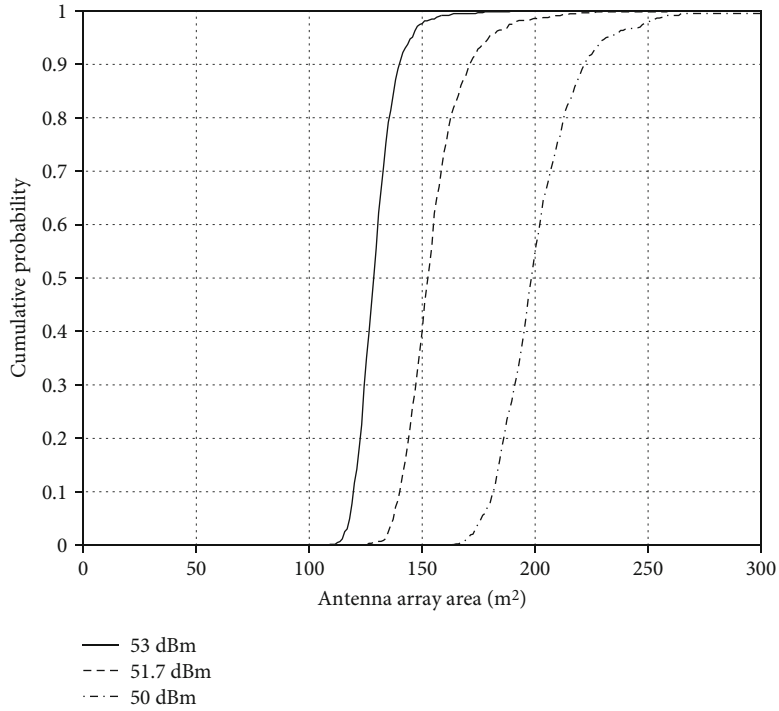

Figure 10: Cumulative probability of users, within the radius of 70 km, experiencing downlink throughput of 30 Mbits/s/terminal where $f_c = 700$ MHz, for different downlink power of 50, 51.7, and 53 dBm.

and τ_{ul} and τ_{dl} represent the number of samples in the coherence block used, respectively, for uplink and downlink data transmission. Sum throughput is calculated as

$$\text{Throughput} = B \times \text{Spectral efficiency}, \tag{19}$$

where B is the available bandwidth.

2.5. Power Control Coefficients. In this paper, we assume max-min fairness power control, meaning maximizing the worst terminal performance and having the same SINR on all terminal. The max-min fairness results in the following optimization problem [11, 12]:

$$\begin{aligned} &\text{maximize} && \bar{\text{SINR}} \\ &\text{with respect to} && \{\eta_u\} \\ &\text{subject to} && (i)\text{SINR}_u \geq \bar{\text{SINR}}, \quad u = 1, \cdots, U \\ & && (ii) 0 \leq \eta_u^{ul} \leq 1 \quad \text{and} \quad \sum_{u=1}^{U} \eta_u^{dl} \leq 1, \end{aligned} \tag{20}$$

where $\bar{\text{SINR}}$ is the average SINR. Power control coefficients become [11, 12]:

$$\eta_u^{ul} = \frac{\min_{u'} \left\{ \gamma_{u'} \right\}}{\gamma_u}, \tag{21}$$

$$\eta_u^{dl} = \frac{1 + \rho_{dl}(\beta_u - \gamma_u)}{\rho_{dl}\gamma_u \left(1/\rho_{dl} \sum_{u'=1}^{U} \left(1/\gamma_{u'} \right) + \sum_{u'=1}^{U} \left(\beta_{u'} - \gamma_{u'}/\gamma_{u'} \right) \right)}. \tag{22}$$

Coherence block in a rural area is large which accommodates a long pilot sequence duration, τ_p. It means enough resource is available to accurately estimate the channel, and thus, we assume the channel estimates are very accurate $\gamma_u \approx \beta_u$. Therefore, (15) and (16) become

$$SINR_u^{UL} = (M - U)\rho_{ul} \min_{u'} \{\beta_{u'}\}, \tag{23}$$

$$SINR_u^{DL} = \frac{(M - U)\rho_{dl}}{\sum_{u'=1}^{U} \left(1/\beta_{u'} \right)}. \tag{24}$$

Later, in Section IV, we use the uplink and downlink SINR expressions in (22) and (23) to evaluate the system performance.

3. Antenna Array Area

It is usually believed that a lower carrier frequency is a better choice for communication in rural area due to lower path-loss and therefore, higher signal range [17]. While this is a fact in one-antenna systems, in massive-MIMO system, one of the major limiting factors is the effective area dedicated to an antenna array and not the carrier frequency. It is shown in [18] that as long as the effective antenna area is fixed, the overall path-loss effect is frequency independent. Moreover,

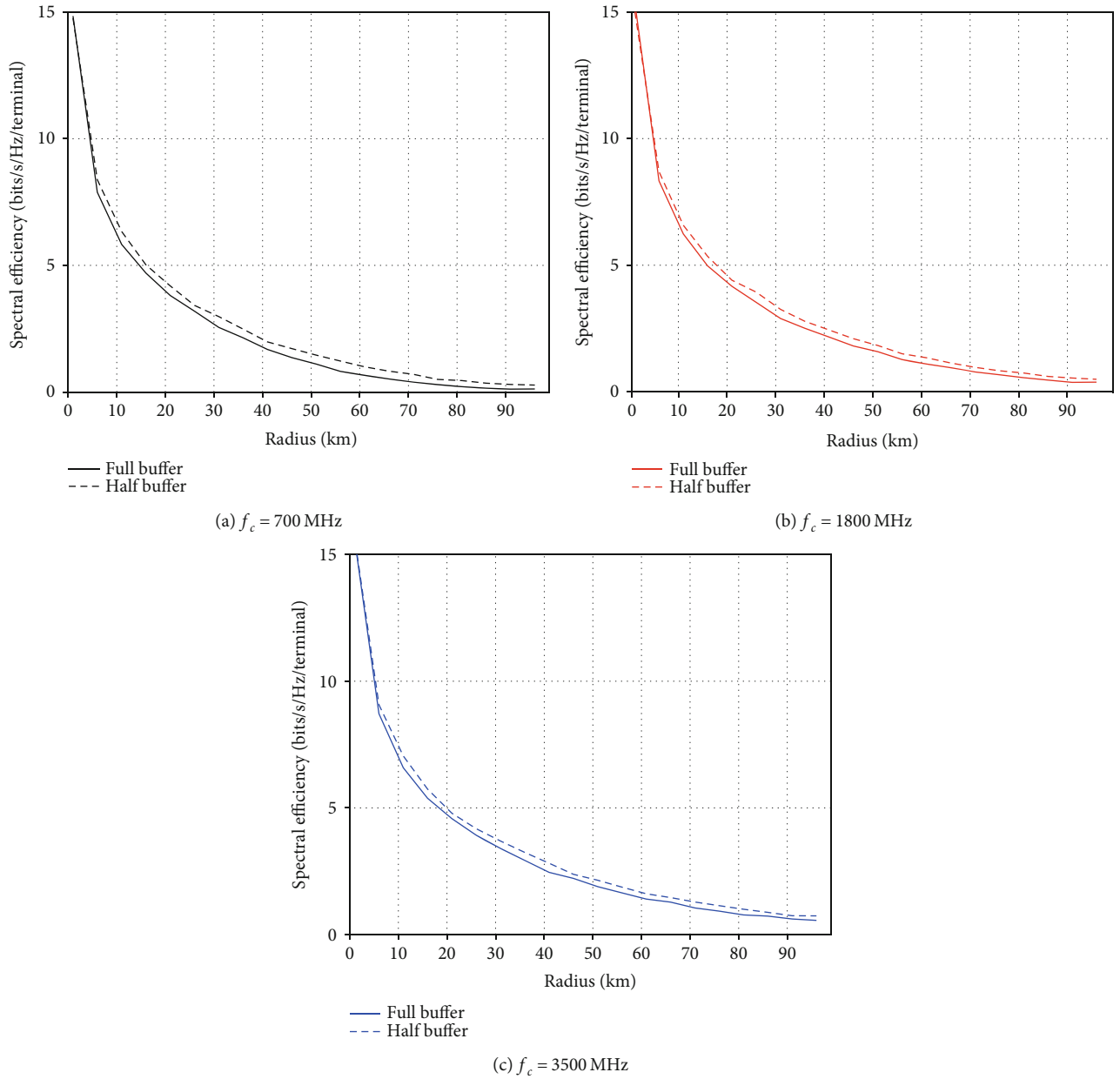

Figure 11: Spectral efficiency improvement in half-buffer condition compared to full-buffer in the uplink.

the cost of an antenna array is an economical factor and will be further reduced by advancing the technology over time; however, the antenna area is a physical limitation that we have to always deal with. Thus, in this work, we fix the antenna array area size, A, and fill it with the maximum possible number of omnidirectional antennas that can fit within for each carrier frequency.

Omnidirectional antennas come in different sizes. In this paper, we assume that the size of an antenna operating in wavelength of λ is $(\lambda/2) \times (\lambda/2)$ where

$$\lambda = \frac{c}{f_c}, \tag{25}$$

where c is the light speed and f_c is the carrier frequency. Considering dual-polarized antenna elements in the array which enables doubling the number of antenna elements on a physical area, we can calculate the maximum possible number of base station antennas, M, filling the fixed antenna array area, A, for a certain carrier frequency. Here, we assume a cylindrical array with radius of $r = 2$ m. This radius allows for 58, 150, and 293 columns of arrays operating in carrier frequency of 700, 1800, and 3500 MHz, respectively. Table 1 shows the number of antennas in each column where the antenna array area is 40, 100, and 125 m^2. In this paper, the element spacing is chosen to be the half of the wavelength, and antenna elements are assuming to be omnidirectional. Figure 3 shows one of the possible configurations where antenna elements, in neighboring bins, do not touch each other. The impact of massive MIMO antenna topologies

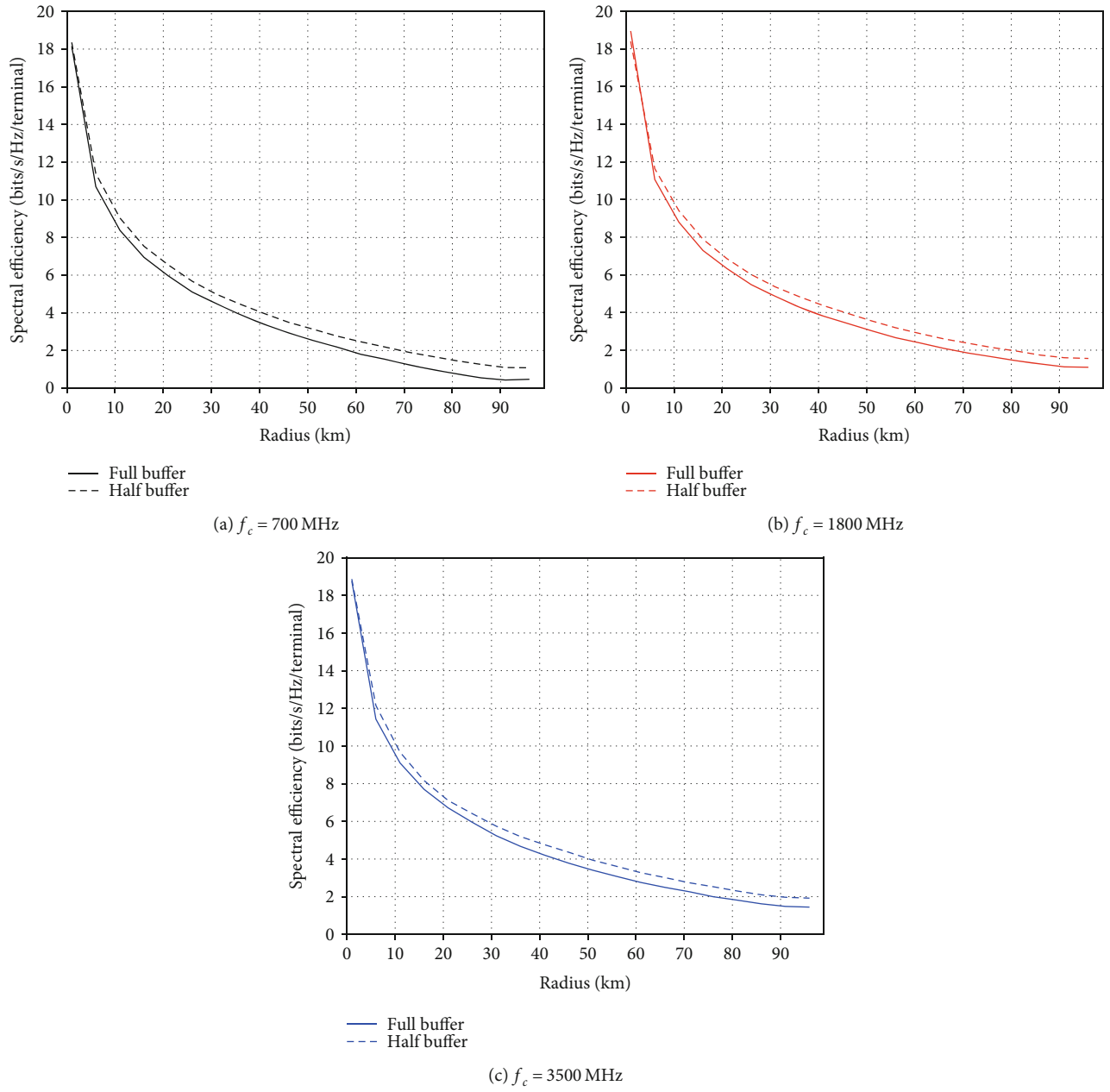

Figure 12: Spectral efficiency improvement in half-buffer condition compared to full-buffer in the downlink.

of cylindrical and rectangular is negligible [19]. In this paper, we assume omnidirectional antennas. Other types of antennas may reduce the number of antennas needed, for example, if users use directive antennas. In the evaluations in Section IV, we assume a cylindrical antenna array with $A \approx 125\,\text{m}^2$ as in Figure 4.

There are some studies on the required antenna separation in rural areas, for instance [21, 22]. These studies show that antenna distance depends on the channel correlation. In this paper, we assume the distance of one-half wavelength between antenna elements in the array [12]. This element spacing can be used in some real antenna arrays, e.g., linear arrays with dipole elements. But, e.g., in microstrip patch antenna arrays, the distance between the elements is typically larger than the half of the wavelength.

4. Simulations

In this paper, we consider a TV tower located 250 m above the ground. We assume HPUE-class (high power user with a radiated power of 31 dBm). Each subscriber is equipped with one antenna, 8 m height with gain of 6 dBi. Later, we also investigate the antenna diversity by assuming two uncorrelated antennas at the user side which provide best of two diversity for shadow fading. Spectral bandwidth is $B = 20$ MHz. Table 2 summarizes the parameters used in our design.

The density of households (users) is assumed to be 0.15 households/km^2. We assume uniform distribution of users, and the results are averaged over large number of random realizations. In our simulation, we only consider the ZF

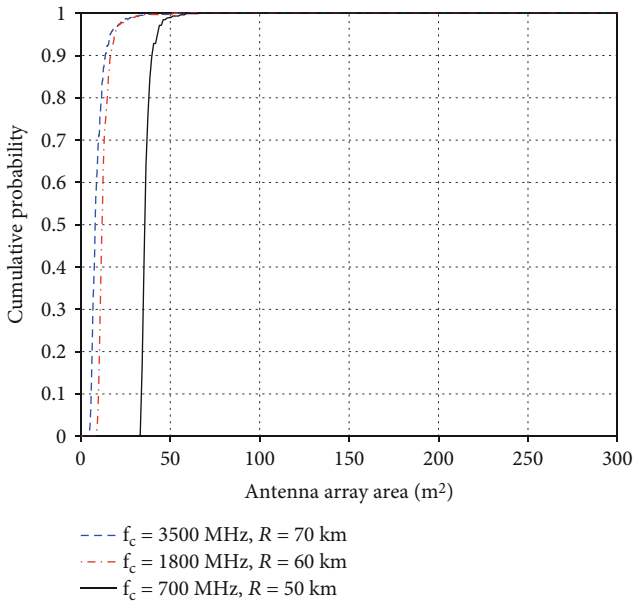

FIGURE 13: Required antenna array area to ensure uplink throughput of 15 Mbits/s/terminal, with different probability, while each household is equipped with two uncorrelated antennas.

operation. Assuming the high-quality channel estimation $\gamma_u \approx \beta_u$, the max-min fairness power control is applied meaning ensuring all terminals experience the same SINR which is equal to the average SINR, see (22) and (23).

In our evaluation, we use (18) and (19) for spectral efficiency and throughput, respectively. We limit the uplink pilot overhead to the number of terminals and assume that each terminal is assigned to a unique orthogonal pilot sequence, $\tau_p = U$. The pilot overhead leaves $(\tau_c - \tau_p)$ of coherence block for data transmission. We split the resources for uplink and downlink transmission as $\tau_{ul} = \tau_{dl} = 1/2(\tau_c - \tau_p)$. The goal is to provide each rural subscriber within the radius of 70 km with downlink throughput of 30 Mbits/s (spectral of sufficiency of 3/2 bits/s/Hz for each subscriber) and uplink throughput of 15 Mbits/s (spectral of sufficiency of 3/4 bits/s/Hz for each subscriber).

With spectrum congestion in recent years, it is important to find a proper bandwidth to use for rural connectivity.

Here, we look at three different frequencies of 700 MHz, available due to shifting from analogue to digital TV [23], 1800 MHz, and 3500 MHz. We also assume that the system works on TDD mode.

Figure 5 shows the probability of all users experience the uplink throughput of 15 Mbits/s within different radius, R, operating on three carrier frequencies of 700, 1800, and 3500 MHz. The antenna array is fixed to a cylinder with radius of 2 m and height of 10 m as depicted in Figure 4, $A \approx 125\,\text{m}^2$. Based on the results in Figure 5 with probability of 85 percent, we can deliver the target uplink spectral efficiency of 3/4 bits/s/Hz (equivalently throughput of 15 Mbits/s) to each terminal within maximum radius of 50 km (1360 households), 60 km (1900 households), and 70 km (2500 households), operating, respectively, on carrier frequency of 700, 1800, and 3500 MHZ. For a fixed antenna array area, A, spectral efficiency is higher in higher frequencies, and thus, we can deliver a certain spectral efficiency to farther distance using higher carrier frequencies. The reason is that more number of antennas increases the beam-forming degrees of freedom, shaping the transmitted beams more precisely. Thus, while, the overall effect of path-loss is the same for all frequencies (since antenna array area is kept the same for all frequencies); in a higher frequency, beams have more power and can reach farther away.

Figure 6 shows the probability histogram of different spectral efficiency for 10000 realization of user distribution within the radius of $R = 60$ km operating at carrier frequency of 1800 MHz. Figure 6, similar to the result from Figure 5, shows that in 85 percent of realizations uplink throughput is at least 15 Mbits/s/terminal.

To ensure that more subscribers will experience the target throughput more antennas, therefore, a larger antenna area is required. Figure 7 examines the uplink throughput of 15 Mbits/s/terminal in a given radius of 50 km (1360 households), 60 km (1900 households), and 70 km (2500 households) for carrier frequencies of 700, 1800, and 3500 MHz, respectively (the points specifically shown in Figure 5). Figure 7 shows that by utilizing $A = 125\,\text{m}^2$, in only around 85 percent of the situations (realizations), the uplink throughput is at least 15 Mbits/s; while more antenna array area is needed to ensure the target throughput in higher percentage of the situations.

Now, we look at the downlink and the target downlink throughput is considered as 30 Mbits/s on all terminals. Figure 8 shows the probability of all users experience the downlink throughput of, at least, 30 Mbits/s within different radius, R, operating on three carrier frequencies of 700, 1800, and 3500 MHz, $A = 125\,\text{m}^2$. We see that with probability of 85 percent, we can deliver the target uplink spectral efficiency of 3/2 bits/s/Hz (equivalently throughput of 30 Mbits/s) to each terminal within maximum radius of 65 km (2190 households), 78 km (3010 households), and 88 km (3670 households), operating, respectively, on carrier frequency of 700, 1800, and 3500 MHz. Figure 9 implies that, similar to uplink, more antenna array area than $A = 125\,\text{m}^2$ is needed to ensure the target throughput in more than 85 percent of situations; however, compared to uplink, the radius of coverage is larger in the downlink.

Moreover, on the downlink, we have the possibility of using high downlink power to achieve a high throughput, and thus, higher downlink power can compensate for small antenna array area as it is depicted in Figure 10. Figure 10 shows the required antenna array area for the target downlink throughput of 30 Mbits/s within the radius of 70 km and $f_c = 700$ MHz, for three downlink power of 50, 51.7, and 53 dBm.

Comparing the presented results of uplink and downlink shows that the system is uplink limited. The antenna array area, which is considered as the cost in this paper, is the common means to achieve the target uplink and downlink throughput. Therefore, the minimum required antenna array area size is $A_{\min} = \max\{A_{\text{ul}}, A_{\text{dl}}\}$, where A_{ul} and A_{dl} are the minimum required antenna area to meet, respectively, the uplink and downlink target throughput within a certain radius. Since the system is uplink limited, $A_{\min} = A_{\text{ul}}$.

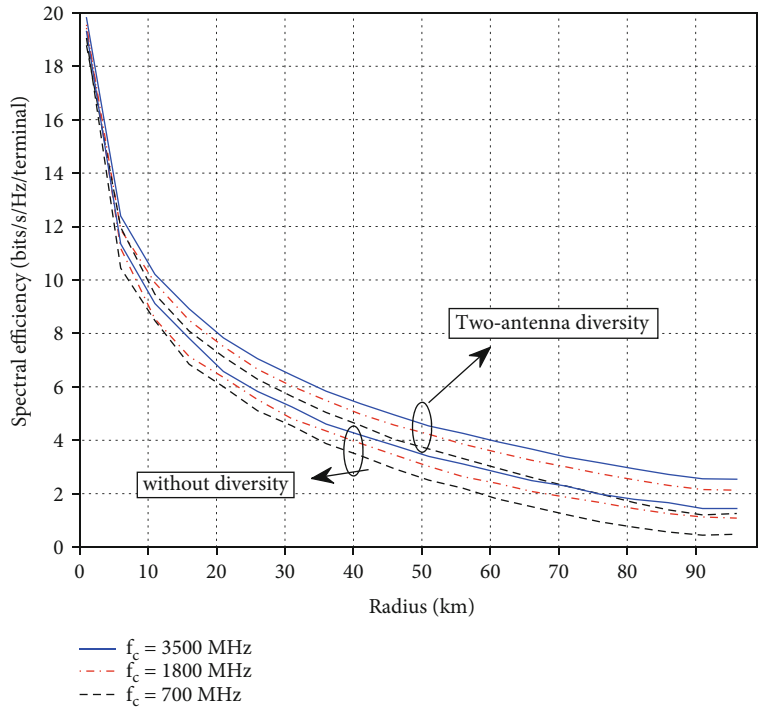

FIGURE 14: Average downlink spectral efficiency utilizing one (no diversity) and two uncorrelated antennas (two-antenna diversity) on each household.

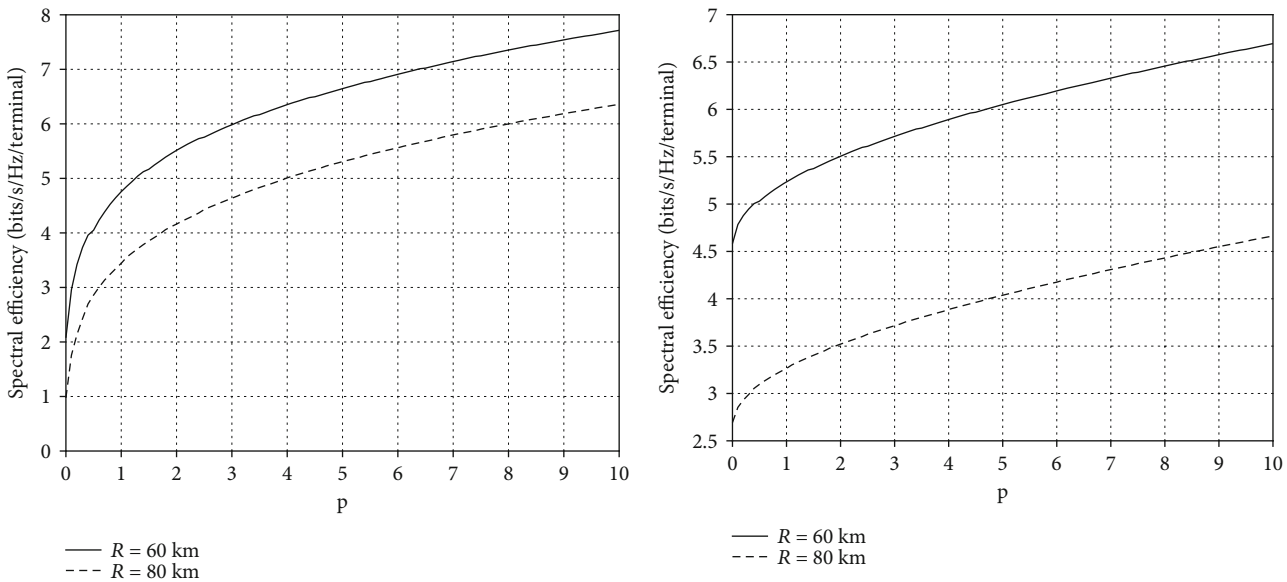

(a) Uplink

(b) Downlink

FIGURE 15: Average spectral efficiency while the p percent of users (the worst conditioned) are dropped, f_c = 1800 MHz.

In our simulations in this paper, we assume that all subscribers are always communicating with maximum bit-rate (full-buffer). However, traffic may be lower at certain time and/or for some subscribers. Considering the lower required traffic, the achievable maximum bit-rate will be higher, or alternatively, we can serve more users and increase the radius of coverage.

Figures 11 and 12 compare the full-buffer condition to half-buffer where only half of the subscribers with maximum bit-rate are communicating.

One way to improve the communication and reduce the effect of shadow fading is to use more than one antenna at each household (user). Here, we consider a diversity of two uncorrelated antennas. Even though full independence of

two antennas is not a realistic assumption, here, we assume the maximum improvement that can happen.

By assuming diversity of best of two, meaning, choosing the better choice of shadow fading effect out of two installed antennas for each user, SF_u in (11) becomes

$$SF_u = \min\left(SF_u^1, SF_u^2\right), \tag{26}$$

where $SF_u^1 \sim \mathcal{LN}(0, 8)$ and $SF_u^2 \sim \mathcal{LN}(0, 8)$ represent the log-normal shadow fading on two possible user's antennas.

By introducing the two uncorrelated antenna diversity, the achievable spectral efficiency within a certain radius increases. Comparing Figures 7 and 13 shows that the introduced diversity reduces the required antenna area to ensure that in almost all situations, we find the max-min fairness solution. In other words, the limitation due to bad conditioned users in terms of shadow fading is decreased.

Adding antenna diversity not only improves the uplink throughput but also improves the downlink throughput. Figure 14 depicts the improvement of average downlink spectral efficiency in the case of two-antenna users over one-antenna user scenario.

In Figure 14, we assume that the two antennas of each user are totally uncorrelated. However, the actual improvement is in between one-antenna diversity curves and two-antenna diversity curves depending on the amount of correlation between antennas.

Max-min fairness power control aims to maximize the minimal throughput; therefore, a very bad conditioned user, for instance, a user with a large shadow fading coefficient, may hugely decrease the performance of the system. Several subscribers may be in hard-to-reach conditions (relatively large β_u) that makes the max-min fairness power control fail to find a solution. To maintain the quality of the service, we can consider to drop some of the worst conditioned users and enhance the quality of the service to the rest of the user terminals. Figure 15 shows that both on uplink and downlink, by dropping some worst users, the average spectral efficiency is improved. The improvement is relatively larger at the beginning when the very worst users are neglected (curves in Figure 15 are steeper at lower percentage).

5. Conclusion

In this paper, we show the feasibility of providing high speed connectivity of 30 Mbits/s to sparse areas, utilizing massive-MIMO. The proposed solution uses the existing infrastructure of high TV towers and can cover radius of 70 km. The system is uplink limited and can be improved by dropping the worst users or equipping users with more than one antenna. The antenna array can be built by stacking column antenna arrays next to each other. For a fixed antenna array area, the number of feasible antennas is larger in higher frequencies giving the opportunity of shaping the beams more precisely; therefore, high frequencies such as 3500 MHz can cover larger areas compared to lower frequencies such as 700 MHz.

Data Availability

No data were used to support this study.

Conflicts of Interest

The authors declare that they have no conflicts of interest.

Acknowledgments

We acknowledge funding by Sweden's innovation agency, Vinnova. The research reported here was carried with support by the #fullcoverage project.

References

[1] "Ericsson website," November 2019, https://www.ericsson.com/en/mobility-report/reports/june-2019/mobile-subscriptions-outlook.

[2] "United nations sustainable development goals," December 2019, https://www.https://www.un.org/sustainabledevelopment/sustainable-development-goals/.

[3] J. Wu, S. Guo, H. Huang, W. Liu, and Y. Xiang, "Information and communications technologies for sustainable development goals: state-of-the-art, needs and perspectives," *IEEE Communications Surveys & Tutorials*, vol. 20, no. 3, pp. 2389–2406, 2018.

[4] J. Beek, M. Bollen, A. Larsson, and M. Eriksson, *Can Solar Power Help Providing Broadband Cellular Coverage in Extreme-Rural Sweden?*, Lulea˚ tekniska universitet, 2016.

[5] "Loon for all," November 2019, http://www.google.com/loon/.

[6] S. Katikala, "Google project loon," *InSight: Rivier Academic Journal*, vol. 10, no. 2, pp. 1–6, 2014.

[7] L. Amorosi, L. Chiaraviglio, F. d'Andreagiovanni, and N. Blefari-Melazzi, "Energy-efficient mission planning of uavs for 5g coverage in rural zones," in *2018 IEEE International Conference on Environmental Engineering (EE)*, pp. 1–9, Milan, Italy, March 2018.

[8] V. Sharma, K. Srinivasan, H.-C. Chao, K.-L. Hua, and W.-H. Cheng, "Intelligent deployment of UAVs in 5G heterogeneous communication environment for improved coverage," *Journal of Network and Computer Applications*, vol. 85, pp. 94–105, 2017.

[9] R. Todd, D. Linton, G. Stafford, and T. Huang, "Multiband reflector antenna for improved satellite communications in rural areas," in *2010 Loughborough Antennas & Propagation Conference*, pp. 469–472, Loughborough, UK, November 2010.

[10] J. Lun, P. Frenger, A. Furuskar, and E. Trojer, "5G new radio for rural broadband: how to achieve long-range coverage on the 3.5 GHz band," in *2019 IEEE 90th Vehicular Technology Conference (VTC2019-Fall)*, pp. 1–6, Honolulu, HI, USA, September 2019.

[11] T. L. Marzetta, *Fundamentals of Massive MIMO*, Cambridge University Press, 2016.

[12] H. Yang and T. L. Marzetta, "Massive mimo with max-min power control in line-of-sight propagation environment," *IEEE Transactions on Communications*, vol. 65, no. 11, pp. 4685–4693, 2017.

[13] J. Milanović, S. Rimac-Drlje, and I. Majerski, "Radio wave propagation mechanisms and empirical models for fixed

wireless access systems," *Tehnički vjesnik*, vol. 17, no. 1, pp. 43–53, 2010.

[14] T. S. Rappaport, "Mobile radio propagation: large-scale path loss," in *Wireless Communications: Principles and Practice*, pp. 107–110, Apprentice Hall, 2002.

[15] H. Asplund, K. Larsson, and P. Okvist, "How typical is the "typical urban" channel model?," in *VTC Spring 2008-IEEE Vehicular Technology Conference*, pp. 340–343, Singapore, Singapore, May 2008.

[16] R. Clarke, "A statistical theory of mobile-radio reception," *Bell System Technical Journal*, vol. 47, no. 6, pp. 957–1000, 1968.

[17] K. Mathew, B. Issac, and T. C. Eng, "A communication architecture using low frequency signals," in *2014 International Conference on Data Science Engineering (ICDSE)*, pp. 188–193, Kochi, India, August 2014.

[18] E. Björnson, J. Hoydis, and L. Sanguinetti, "Massive mimo networks: spectral, energy, and hardware efficiency," *Foundations and Trends® in Signal Processing*, vol. 11, no. 3-4, pp. 154–655, 2017.

[19] C. T. Neil, M. Shafi, P. J. Smith, and P. A. Dmochowski, "On the impact of antenna topologies for massive mimo systems," in *2015 IEEE International Conference on Communications (ICC)*, pp. 2030–2035, London, UK, June 2015.

[20] "Statistics Sweden website," February 2020, https://www.scb.se.

[21] D. Pinchera, M. Migliore, F. Schettino, and G. Panariello, "Antenna arrays for line-of-sight massive mimo: half wavelength is not enough," *Electronics*, vol. 6, no. 3, p. 57, 2017.

[22] P. Chandhar, D. Danev, and E. G. Larsson, "On ergodic rates and optimal array geometry in line-of-sight massive mimo," in *2016 IEEE 17th International Workshop on Signal Processing Advances in Wireless Communications (SPAWC)*, pp. 1–6, Edinburgh, UK, July 2016.

[23] M. Khalil, J. Qadir, O. Onireti, M. A. Imran, and S. Younis, "Feasibility, architecture and cost considerations of using tvws for rural internet access in 5G," in *2017 20th Conference on Innovations in Clouds, Internet and Networks (ICIN)*, pp. 23–30, Paris, France, March 2017.